Available online at www.sciencedirect.com
ScienceDirect
Journal of Photochemistry and Photobiology A: Chemistry 194 (2008) 189–199
Journal of Photochemistry and Photobiology A:Chemistry
www.elsevier.com/locate/jphotochem

A FT-IR (DRIFT) study of the influence of halogen substituents on the TiO_2-assisted photooxidation of phenol and *p*-halophenols under weak room light irradiance

Satoshi Horikoshi [a,b,*], Takashi Miura [a], Masatsugu Kajitani [a], Hisao Hidaka [c], Nick Serpone [d,**]

[a] *Department of Chemistry, Faculty of Science and Technology, Sophia University, 7-1 Kioi-cho, Chiyoda-ku, Tokyo 102-8554, Japan*
[b] *Materials Research Institute for Sustainable Development, National Institute of Advanced Industrial Science and Technology (AIST), 2266 Anagahora, Shimo-Shidami, moriyama-ku, Nagoya, Aichi 463-8560, Japan*
[c] *Frontier Research Center for the Global Environment Science, Meisei University, 2-1-1 Hodokubo, Hino, Tokyo 191-8506, Japan*
[d] *Dipartimento di Chimica Organica, Universita di Pavia, Via Taramelli 10, Pavia 27100, Italy*

Received 18 May 2007; received in revised form 6 August 2007; accepted 6 August 2007
Available online 12 August 2007

Abstract

Early events occurring when *p*-halophenols (*p*-XPhOH; X = F, Cl, Br) and phenol (PhOH) interact with a metal-oxide surface (e.g. TiO_2) through adsorption and/or photoinduced adsorption have been examined by FT-IR diffuse reflectance (DRIFT) spectroscopy. Exposure of *p*-XPhOH/TiO_2 specimens (X = H, F, Cl, Br) to very weak UV light (290–390 nm; $\leq$1.8 $\mu W\,cm^{-2}$) led to significant changes in the C—O stretching band, ν(C—O), in the spectral range 1100–1350 cm^{-1}. A new band emerged at higher frequency with isosbestic points clearly observable, inferring formation of a single intermediate product in all four cases, namely the 4-halocatechols (catechol in the case of phenol). This inference is supported by theoretical MOPAC calculations of point charges and radical frontier electron densities of all the atoms in the original phenolic structures. The TiO_2 photo-assisted degradation (UV irradiance ~0.80 $mW\,cm^{-2}$; UV–vis spectroscopy) and mineralization (evolution of CO_2) of the phenols was also examined in UV-irradiated aqueous dispersions, together with dehalogenation (HPLC ion chromatography). Analyses of process dynamics indicate little variations in the rates of photodegradation (slightly faster for the *p*-BrPhOH/TiO_2 specimen). Photoinduced dehalogenation was nearly complete after ca. 3 h of irradiation with k_X varying as *p*-FPhOH $\gg$ *p*-ClPhOH > *p*-BrPhOH. About 35% of the F^- ions could not be accounted for, as they remained strongly adsorbed on the TiO_2 surface. Evolution of CO_2 was also nearly quantitative but slower than dehalogenation. Within experimental error, k_{CO_2} followed the trend *p*-FPhOH $\geq$ *p*-ClPhOH $\geq$ PhOH $\geq$ *p*-BrPhOH. The influence of F^-, Cl^- and Br^- ions on the dynamics of the TiO_2-assisted photodegradation of phenol was also examined. Results revealed little variation except for the presence of Br^- ions, which caused phenol to photodegrade three times slower. Either the Br^- ions blocked surface active sites or else the bromide ion and the phenol competed for the oxidizing $^{\bullet}OH$ radicals and/or the photogenerated valence band holes.

Keywords: Halophenols; Low-irradiance TiO_2 photooxidations; FTIR-DRIFT spectra; Effect of halogens on photooxidations; Dehalogenation; Point charges; Radical frontier electron densities

1. Introduction

Environmental pollution caused by halogen-bearing chemicals present serious worldwide problems and considerable challenges in meeting objectives to resolve environmental pollution. Significant quantities of polychlorinated phenols of complex structures are typically used in wood preserving indus-

* Corresponding author at: Department of Chemistry, Faculty of Science and Technology, Sophia University, 7-1 Kioi-cho, Chiyoda-ku, Tokyo 102-8554, Japan.
** Co-corresponding author.
E-mail addresses: s-horiko@sophia.ac.jp (S. Horikoshi), nick.serpone@unipv.it, nickser@alcor.concordia.ca (N. Serpone).

1010-6030/$ – see front matter © 2007 Elsevier B.V. All rights reserved.
doi:10.1016/j.jphotochem.2007.08.007

tries in the pressure treatment of wood. Chlorophenol is rather toxic. Accordingly, the decomposition of chlorophenol and, by extrapolation, its congeners is an essential requirement in environmental remediation.

The cleanup of contaminated sites with high loads of halogenated chemicals by bacterial biodegradation methods alone, using activated sludge, presents no insignificant difficulties. Attractive alternatives have been advanced oxidation processes (AOPs) such as UV/H_2O_2, ozonation, UV/O_3, the Fenton and photo-Fenton processes, and not least TiO_2 photo-assisted degradations [1]. The past three decades have witnessed a plethora of studies of chlorophenolic compounds that have been used to evaluate the various AOPs, with the involvement of TiO_2 particulates being particularly noteworthy. Several methodologies were used. Among these were the usage of TiO_2 electrodes [2], TiO_2/surfactant micelles [3], TiO_2-coated fiber optics [4], TiO_2/microwaves [5,6], large scale photoreactors [7], and TiO_2-fixed thin films [8]. Mechanistic details of the photodegradation of chlorophenol [9–16] together with some aspects of surface reactions involving chlorophenol [17–20] have been reported and intermediates identified. The effect of the number and positions of halogen substituents on the phenyl ring on the photodegradation process has similarly been examined in some reports [21–23]. However, studies that examined possible correlation between different halogen substituents and photodegradation efficiency have been somewhat lacking.

The present study focused on examining the photodegradation of *p*-fluorophenol (*p*-FPhOH), *p*-chlorophenol (*p*-ClPhOH), *p*-bromophenol (*p*-BrPhOH), and the parent phenol (PhOH) in UV-irradiated TiO_2 dispersions. The particular emphasis was (i) to probe the early events [24] in the photo-degradative process by FT-IR diffuse reflectance (DRIFT) spectroscopy by exposing the dispersion specimens to very weak UV/visible radiation (irradiance $\leq 1.8\,\mu W\,cm^{-2}$) as might be available in domestic environments, (ii) to examine closely the influence and the nature of the halogen substituents on the extent of initial adsorption process in the dark and possibly on the photoinduced adsorption, and (iii) to explore possible correlations, if any, between theoretically calculated point charges and radical frontier electron densities on all the atoms of the phenolic structures with the experimental dynamics. We also examined the TiO_2 photo-assisted degradation of phenol in the presence of fluoride, chloride and bromide ions to assess how these halides affect this particular AOP in the case of this aromatic substrate.

2. Experimental

2.1. Chemical reagents

High purity grade *p*-chlorophenol, *p*-bromophenol, *p*-fluorophenol and phenol substrates were supplied by Tokyo Kasei Co. Ltd., whereas Degussa P-25 TiO_2 was supplied by Nippon Aerosil Co. Ltd. (particle size, 20–30 nm by TEM observations; 83% anatase and 17% rutile by X-ray diffraction; surface area, $53\,m^2\,g^{-1}$ measured by the BET method).

2.2. Photodegradation procedures

Aqueous suspensions (0.20 mM; 70 mL) containing TiO_2 particles (10 mg) were contained in a 120-mL Pyrex glass photoreactor. Once closed, the photoreactor was purged with pure oxygen for 10 min. The heterogeneous system was subsequently dispersed by sonication for 5 min under dark conditions. Unless otherwise noted, UV irradiation of the dispersions was achieved using a 75-W high-pressure mercury lamp; light irradiance $\sim 0.80\,mW\,cm^{-2}$ in the wavelength range 320–390 nm (maximal emission, $\lambda = 360$ nm). The initial pHs of the dispersions were 6.2 (PhOH), 5.8 (FPhOH), 5.9 (ClPhOH), and 6.1 (BrPhOH), against an isoelectric point of ca. 6.5 for P-25 TiO_2 determined by the zeta potential method.

The influence of F^-, Cl^-, and Br^- ions on the photodegradation of phenol was also examined. Aqueous solutions (35 mL; 0.40 mM in the phenols) of FPhOH, ClPhOH, and BrPhOH containing TiO_2 particles (10 mg) were introduced into a 120-mL Pyrex glass photoreactor (initial pHs of the dispersions are reported in Section 3). Once closed, the photoreactor was purged with pure oxygen for ca. 10 min, followed by sonication for 5 min under dark conditions. The dispersion was then UV-irradiated continuously for ca. 24 h with the 75-W high-pressure Hg lamp (irradiance, ca. $0.80\,mW\,cm^{-2}$), subsequent to which the organic carbon in the halophenols was completely converted to CO_2 gas. Analyses indicated that the principal components left in the aqueous dispersions were the TiO_2 particles and the free F^-, Cl^-, and Br^- ions. To these dispersions was then added an aqueous phenol solution (35 mL; 0.40 mM) bringing the aqueous dispersions to contain phenol (70 mL; 0.20 mM) and the relevant F^-, Cl^-, and Br^- ions (0.20 mM) together with TiO_2 particles (10 mg).

Adsorption of F^-, Cl^-, and Br^- ions on the TiO_2 particles (10 mg) was examined using respective NaX (X = F, Cl, Br; 0.20 mM) aqueous salt solutions in the Pyrex glass reactor under dark conditions. Interactions of halide ions with the metal-oxide particle surface were examined in aqueous TiO_2 dispersions with NaCl (pH 5.7), NaBr (pH 5.6) and NaF (pH 5.5) under otherwise similar dark and UV-light irradiation conditions. The suspensions were first purged with pure oxygen and then dispersed by sonication for 5 min, followed by stirring for 30 min under dark conditions to determine the extent of adsorption of the halides on the metal-oxide surface. Subsequently, the dispersions were UV-light irradiated to assess the extent of photoadsorption. Concentration changes of the halide ions were measured by ion chromatography.

2.3. Analytical methods

DRIFT spectra were recorded on a JASCO FT/IR-6100 spectrometer equipped with a diffuse reflectance attachment. The samples, consisting of a paste composed of TiO_2 powder (20 mg) and a saturated aqueous solution of the phenols, were exposed for ca. 10 min to very weak UV-light from the laboratory ceiling fluorescent lamps (wavelengths, 290–390 nm; irradiance, $\leq 1.8\,\mu W\,cm^{-2}$) during which the DRIFT spectra were recorded at various intervals. A UV–vis spectrophotometer (Shimadzu

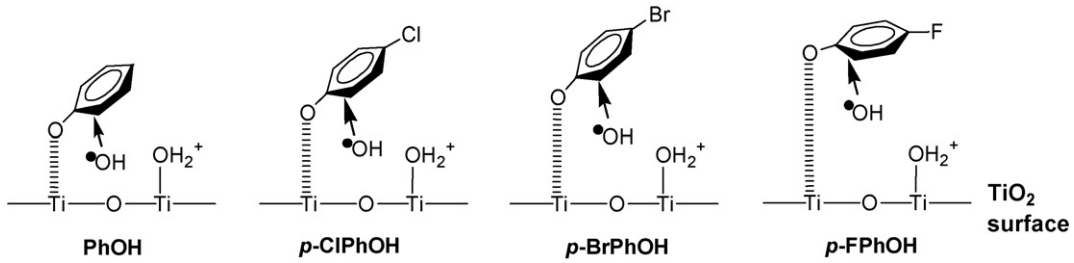

Scheme 1. Schematic images of the possible mode of adsorption of the substrates on the TiO_2 particle surface and potential attack by the photogenerated •OH radicals at the positions indicated.

UV-2500PC; double monochromator detection system) monitored the degradation of the phenols through disappearance of the absorption features of the benzene ring at appropriate wavelengths. TiO_2 photo-assisted dehalogenation of the halophenols was assayed by ion chromatography using a JASCO LC-2000 Plus HPLC Chromatograph equipped with a conductivity detector and an I-524 anionic column. The temporal evolution of CO_2 that attested to the photomineralization of the phenols was monitored by gas chromatography (Hitachi 263-30; TCD detector; Porapack Q column; column temperature, 50 °C). Helium was the carrier gas. The amount of carbon dioxide evolved was quantified by a pre-determined calibration curve. The 200-μL sample in the headspace volume of the vessel after photodegradation was taken up with a microsyringe.

2.4. Theoretical MOPAC calculations

Molecular orbital calculations were performed on a personal computer using the MOPAC version 6 software package (Fujitsu Co. Ltd.). Point charges were calculated for an optimized geometry of the phenols in aqueous media using the Augmented MM2 optimization method that was then followed by the MOPAC (with AM1 parameters) and the conductor-like screening model (COSMO) methodology [25]. The atoms were identified according to the structure below. The initial positions of possible •OH-radical attack of the phenolic structures were estimated from calculations of radical frontier electron densities (RFED). The corresponding RFEDs of the transition-state geometries were also determined for all atoms of the *p*-halophenols and phenol after optimizing the molecular geometries:

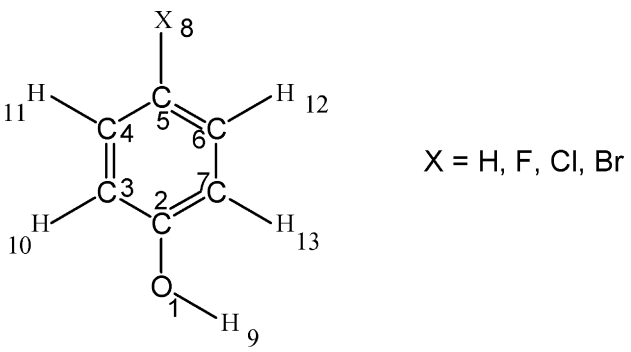

using MOPAC with AM1 parameters and the COSMO software. A complete set of point charges and radical frontier electron densities of all atoms in the phenolic structures are available upon request [26].

3. Results and discussion

3.1. Calculated point charges and radical frontier electron densities

Molecular structure and atomic charge calculations for *p*-fluorophenol, *p*-chlorophenol, *p*-bromophenol and phenol using MP2 and density functional (B3LYP) methods with the extended 6–311++G(df, pd) basis set were reported recently [27,28]. Structural changes of the phenyl ring seem to be governed mainly by the electronegativity of the halogen substituents X, with the inductive effect being greatest for fluorine. Resonance effects induced by both the OH and X substituents at the *para* position also contribute to the geometrical changes of the phenyl ring. Although the atomic charges on the non-hydrogen atoms reported earlier [27,28] differ from the point charges determined in the present study [26] because of the different calculation methodology (MOPAC), the trends are nevertheless similar.

As expected from the OH group resonance effect in PhOH, the (negative) point charges are greatest at the *ortho* (*C3*, −0.198; *C7*, −0.227) and *para* (*C5*, −0.198) positions relative to those at positions *meta* (*C4*, −0.116; *C6*, −0.114) to the OH group. Particularly interesting is that such effects places a positive point charge at the *C2*–OH carbon atom (+0.071) in phenol, as also occurs for the *C2* carbons in the three *p*-halophenols with charges ranging from +0.070 to +0.102 (Br > Cl > H ∼ F). Of greater import are the effects of the halogen substituents on the magnitude of the point charges on the overall structures.

Bonding of an electronegative halogen to the *C5*–X carbon atom brings about a significant alteration of the charge on this carbon, which ranges from +0.025 in *p*-FPhOH to −0.251 in *p*-BrPhOH with the order being *p*-FPhOH > *p*-ClPhOH > PhOH > *p*-BrPhOH. In the *p*-FPhOH case, the positive charge on *C5* (+0.025) is accompanied by an increase of the negative charges on the *C4* (−0.137) and *C6* (−0.135) atoms relative to those on PhOH, whereas a large negative charge on the *C5* carbon (−0.251), the case for *p*-BrPhOH, brings about a decrease of the negative charge at *C4* (−0.073) and *C6* (−0.074) relative to PhOH. The inductive effect is obviously greatest for the F substituent and least for Br followed by Cl; this trend correlates with the electronegativity of the halogens: F (4.1) > Cl (2.83) ≥ Br (2.74). The largest negative charges on the non-

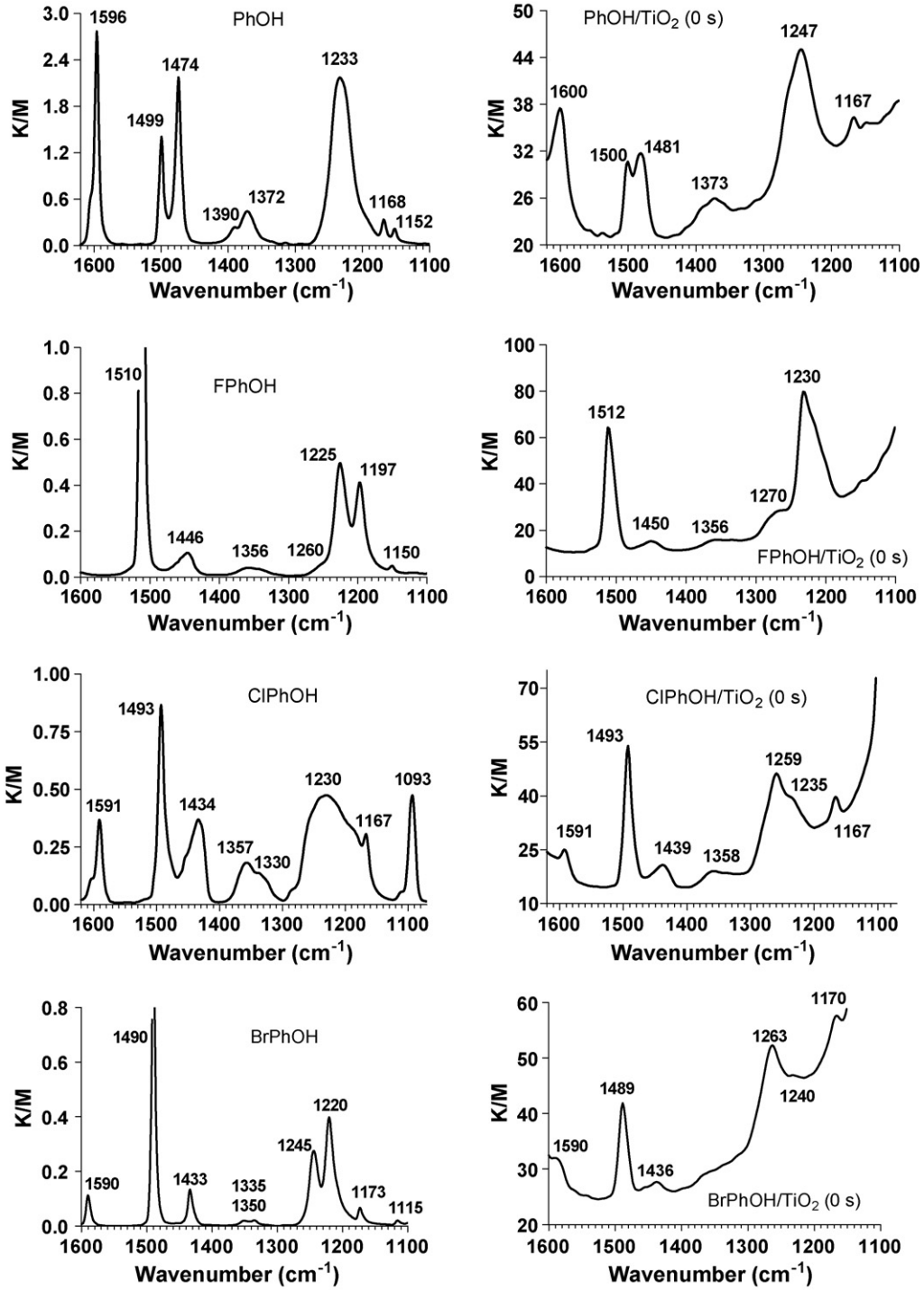

Fig. 1. DRIFT spectra of the *p*-halophenols and phenol in the spectral range 1100–1600 cm^{-1} (except for *p*-ClPhOH—see text) and DRIFT spectra of the *p*-XPhOH/TiO_2 pastes consisting of a saturated phenolic solution and TiO_2 powder in the dark at $t = 0$ s (see text for additional details).

hydrogen atoms of the phenolic structures reside on the *O1* atom (ca. −0.317 to −0.320) of the *C2*–O–H fragment followed by the *C7* carbon (−0.198 to −0.227). This has significant consequences on the mode with which PhOH and the three *p*-XPhOH phenols are adsorbed on the TiO_2 particle surface. On the basis of calculated point charges then we infer the mode of adsorption of the phenolic substrates to be as illustrated in the models of Scheme 1.

Comparison of the point charges on the aromatic ring structures also reveals an asymmetric distribution of the charges at the two carbon atoms *ortho* to the OH group position. That is, the *C7* carbon atom in all the ring structures have a greater negative charge than their analogous *C3* carbons (−0.198 to −0.227 versus −0.168 to −0.198). This is undoubtedly caused by the O–H groups pointing toward the *C7* atoms (see structure above), a point also made by Zienkiewicz and coworkers

[27,28]. These workers also examined experimentally (in the inert solvents CCl_4 and cyclohexane) and theoretically calculated infrared spectra of the *p*-XPhOH (X = H, F, Cl, Br) substrates using the B3LYP method with the 6–311++G(df, pd) basis set. Their results led to unequivocal assignments of experimental IR spectral bands on the basis of calculated potential energy distributions. Similar studies were reported by Wiest and coworkers [29], albeit on quinoline and 2,4-dichlorophenoxy acetic acid.

The radical frontier electron densities that are of particular interest in assessing the position(s) of •OH-radical attack of the phenols display somewhat different aspects about the role of inductive and resonance effects in these phenolic species. Indeed, the largest electron densities are seen on the *C2* and *C5 para* carbon atoms with values ranging from 0.369 on PhOH to 0.457 on *p*-BrPhOH [26], making these two positions the more likely ones to be subjected to an •OH-radical attack (see Scheme 1). The two carbon atoms *ortho* to the C–OH group (i.e. *C3* and *C7*) bear the next highest radical frontier electron densities (0.226–0.303), followed by the *C4* and *C6* carbons (0.210–0.254).

3.2. Initial events occurring on the TiO_2 surface involving *p*-XPhOH (X = H, F, Cl, Br) molecules—a FT-IR study

The diffuse reflectance Fourier transform infrared (DRIFT) and angular total reflection Fourier transform infrared (ATR-FTIR) methodologies have been shown to be useful techniques [30,31] with which to probe the mode(s) of adsorption of organic substrates [32–34] and the evolving formation of primary intermediates [24] on such metal-oxide surfaces as those of the anatase and rutile TiO_2 polymorphs. It was not the goal of the present study to probe the details of the pH effect as it might impact on the adsorption mode(s) [34,35]. Rather, the primary goal was to probe the sequential events that occur on the metal-oxide surface in the first few minutes of irradiation [24,36]. Accordingly, we used the DRIFT spectroscopic technique to ascertain what the mode of adsorption, if any, of the halophenols and phenol on the TiO_2 particle surface might be under the prevailing conditions. The sample was typically a paste consisting of 20 mg TiO_2 and a saturated solution of the phenols. DRIFT spectra of the *p*-XPhOH/TiO_2 samples were recorded before irradiation and then under irradiation with the samples exposed to the very weak radiation emitted by laboratory fluorescent ceiling lamps (290–390 nm; maximal emission, 340 nm; UV irradiance $\leq 1.8\ \mu W\ cm^{-2}$) for a total of about 600 s at 20-s (X = H, F, Br) or 35-s (X = Cl) intervals. Note that the sample housing in the FT-IR spectrophotometer was an open chamber, which allowed the samples to be thus subjected to the laboratory radiation.

Fig. 1 reports the DRIFT spectra of the TiO_2-free phenolic solutions in the range 1100–1600 cm^{-1} (except for *p*-ClPhOH) together with the corresponding spectra of the *p*-XPhOH/TiO_2 specimens at time 0 s (dark). Note that the liquid nature of *p*-ClPhOH precluded a DRIFT spectrum. Accordingly, for this halophenol we report a converted normal transmittance IR spectrum {Kubelka–Munk type spectrum by a computer software}

Table 1
Summary of FT-IR diffuse reflectance vibrational band positions for the three *p*-halophenols and phenol in the range 1100–1600 cm^{-1} together with the phenols deposited on the TiO_2 particle surface in the dark (time = 0 s; see text for details)

PhOH	PhOH/TiO_2 (dark)	FPhOH	FPhOH/TiO_2 (dark)	ClPhOH	ClPhOH/TiO_2 (dark)	BrPhOH	BrPhOH/TiO_2 (dark)	Major components
– (1069)	–	–	–	1093 (1102)	–	1115 (1102)	–	ν(C–C) + ν(C–X)
1152 (1161)	–	1150 (1155)	–	–	–	–	–	δ(C–H)
1168 (1175)	1167	1197 (1167)	–	1167 (1164, 1171)	1167	1173 (1164, 1173)	1170	δ(O–H), δ(C–H)
–	–	1225 (1221)	1230	–	–	–		ν(C–F)
1233 (1260) very strong	1247, 1264	1260 (1265) very weak sh.	1265	1230 (–) very broad	1235, 1259	1220, 1245 strong (1260)	1240, 1263	ν(C–O) + ν(C–C)
– (1326)	–	– (1299)	–	1330 (1328)	–	1335 (1327)	–	δ(C–H) + ν(C–C)
1372, 1390 (1350)	1373	1356 (1335)	1356	1357 (–)	1358	1350	–	ν(C–C)
1474 (1479)	1481	1446 (1446)	1450	1434 (1430)	1439	1433 (1427)	1436	ν(C–C)
1499 (1506)	1500	1510 (1519)	1512	1493 (1497)	1493	1490 (1493)	1489	δ(C–H) + ν(C–C)
1596 (1609)	1600	– (1618)	–	1591 (1597)	1591	1590 (1594)	1590	ν(C–C)

Suggested assignments and calculated IR band positions in parentheses for phenol and the *p*-halophenols [27,28,37].

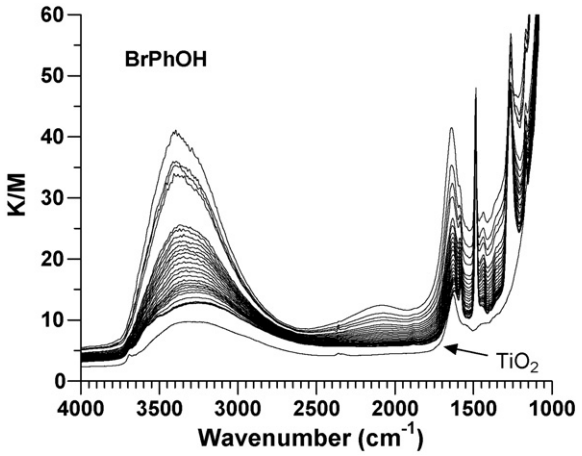

Fig. 2. Temporal spectral changes occurring in the DRIFT spectra in the *p*-BrPhOH/TiO_2 sample in the 1000–4000 cm^{-1} range; the spectrum for TiO_2 alone is also shown for comparison.

taken with KBr cells. Infrared band positions are summarized in Table 1, along with assignments to various vibrational modes [27,28]. Fig. 2 displays the full DRIFT spectrum of the *p*-BrPhOH/TiO_2 specimen between 1000 and 4000 cm^{-1}, which reveals the temporal conversion of the phenol to some intermediate product(s). Fig. 3 focuses on the spectral changes occurring in the region 1200–1350 cm^{-1} for the *p*-XPhOH/TiO_2 specimens (X = H, F, Cl, Br).

The C–F stretching vibration contributes significantly to the strong band observed at 1225 cm^{-1} in *p*-FPhOH, whereas the slightly weaker band at 1197 cm^{-1} is due to a combination band involving in-plane bending of the phenyl ring and stretching vibrations of the C–F and C–O bonds. The in-plane bending O–H mode contributes to the 1356 cm^{-1} band and likely also to the band at 1446 cm^{-1} for *p*-FPhOH. The corresponding bands in the spectra of *p*-ClPhOH occur at 1167, 1330, and 1434 cm^{-1}, whereas in *p*-BrPhOH they are seen at 1173, 1335, and 1433 cm^{-1}. For PhOH, these bands occur at 1168 and 1372 cm^{-1}; see also Ref. [37]. In the *p*-XPhOH/TiO_2 specimens, these infrared bands do not shift to any great extent (see Table 1), at least at time 0 s (Fig. 1). The ν(C–F) stretching vibration contributes strongly to the significant IR band at 1230 cm^{-1}. Analogous, relatively strong ν(C–Cl) and weak ν(C–Br) bands in the IR spectra of *p*-ClPhOH and *p*-BrPhOH occur at somewhat lower frequencies, 1093 and 1115 cm^{-1}, respectively, although ν(C–C) stretching vibrations also contribute to these bands [27,28]. The latter two carbon–halogen stretching bands are not seen in the IR spectra of the *p*-ClPhOH/TiO_2 and *p*-BrPhOH/TiO_2 specimens as they are masked by the very strong signals below 1100 cm^{-1} of the TiO_2 support [38].

The unusually weak band (shoulder) at 1260 cm^{-1} in the IR spectrum of *p*-FPhOH involves predominantly a contribution from the ν(C–O) stretching mode and to some extent the ν(C–C) vibrations [27]. By contrast, the analogous band in phenol at 1233 cm^{-1} is rather strong. The corresponding C–O stretch-

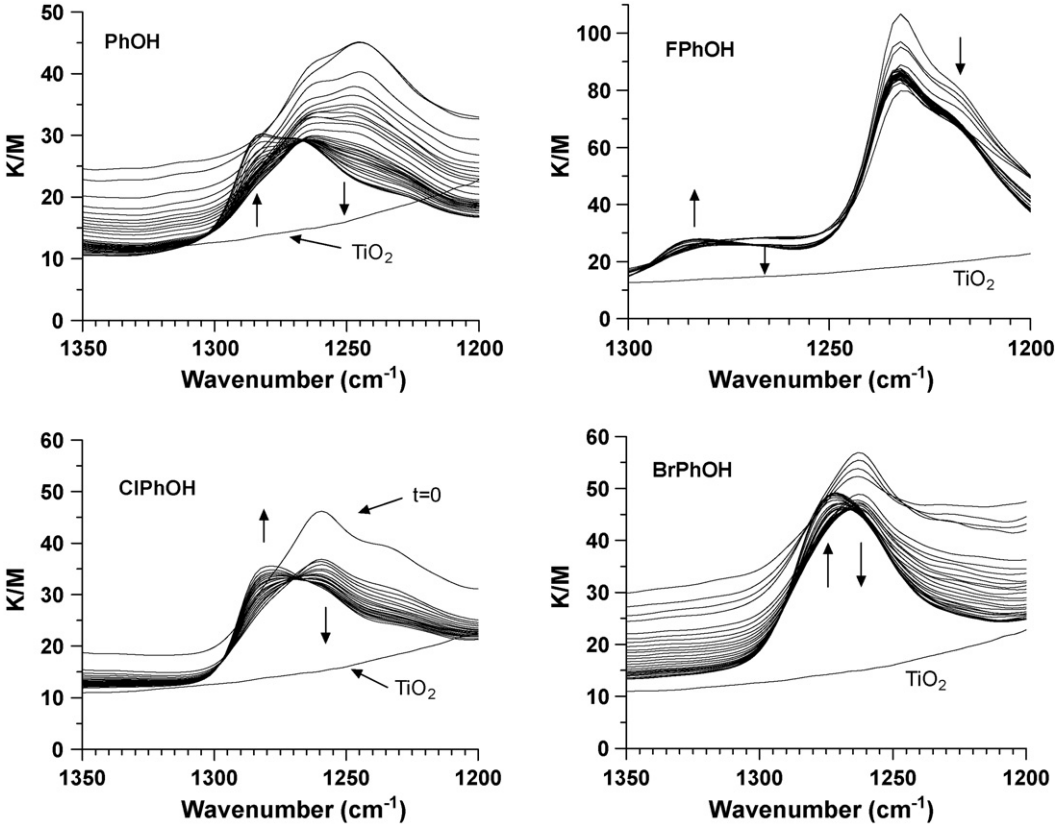

Fig. 3. Expanded view of the DRIFT spectra in the range 1200–1350 cm^{-1} of the *p*-XPhOH/TiO_2 specimens as a function of time illustrating the changes taking place under very weak irradiation conditions (see text for details).

ing vibration in the IR spectra of *p*-ClPhOH and *p*-BrPhOH species is observed at 1230 cm^{-1} (X = Cl), and at 1220 and 1245 cm^{-1} (X = Br), in relatively fair agreement with theoretical estimates [27,28,37]. In the *p*-XPhOH/TiO_2 systems, these bands are shifted to higher frequency by 5 to 30 cm^{-1}, i.e. to 1247 cm^{-1} and 1264 cm^{-1} for PhOH/TiO_2, to 1265 cm^{-1} for *p*-FPhOH/TiO_2, to 1235 and 1259 cm^{-1} for *p*-ClPhOH/TiO_2, and to 1240 and 1263 cm^{-1} for *p*-BrPhOH/TiO_2. It is the latter ν(C–O) vibrational bands that are of most interest in assessing the early events occurring on the TiO_2 particle surface when the *p*-XPhOH/TiO_2 systems are irradiated (see Figs. 2 and 3).

Carbon–hydrogen bending modes, δ(C–H), contribute extensively [27,28,37] to the many bands seen in Fig. 1 with the foremost and strongest band occurring in the 1490–1510 cm^{-1} spectral range. These bending modes are not affected when the phenolic species are deposited on the TiO_2 particle surface. The bands in the above range also originate in part from C–C stretching vibrations, i.e. from phenyl ring vibrations.

Changes observed in the ν(C–O) bands in the spectra of Fig. 1 (see also Table 1) between the free *p*-XPhOH molecules and the *p*-XPhOH/TiO_2 systems, together with the relatively large negative point charges on the oxygen atoms [26], suggest that the phenolic species are chemisorbed on the metal-oxide surface through a heterolytic dissociative pathway and are likely tilted [39] in the manner proposed in the models of Scheme 1. The extent of the tilt was inferred from the point charges of the halogens [26] and from their electronegativities (Table 2). The shift to a higher frequency for these ν(C–O) vibrational modes indicates some increase in the C–O force constant when the phenols interact with the particle surface. The (sudden) drop in the intensity of the bands for the *p*-XPhOH/TiO_2 systems after the first 20–35 s irradiation period (fluorescent lamp illumination) that these systems are subjected to indicates that photoadsorption may also be involved in *stabilizing* the adsorbates on the metal-oxide surface. In this regard, the temporal spectral changes illustrated for *p*-BrPhOH/TiO_2 in Fig. 2 are quite revealing; similar changes were observed for the other systems. A steady decrease in the intensity of the bands occurs across the whole range reported, which approaches the IR spectrum of the TiO_2 photomediator after ca. 10 min (600 s). Most remarkable are the changes occurring in the spectral region where the C–O stretching mode makes its strongest contribution to the overall IR spectra. The expanded view (1200–1350 cm^{-1}) of these changes is reported in Fig. 3 for all four systems.

For PhOH/TiO_2, the 1247 and 1264 cm^{-1} bands decrease in intensity for ca. 240 s, following which a new infrared band begins to emerge at 1283 cm^{-1} with isosbestic points at 1267 and 1302 cm^{-1} maintained up to 600 s. We infer that the first process is continued photoadsorption of PhOH with loss in intensity of the bands owing to the more constrained structure of phenol as the adsorbate on TiO_2. The process beginning at 240 s, however, clearly demonstrates that the phenol is converted to a single intermediate with band at 1283 cm^{-1} and with the complete loss of the 1247 cm^{-1} band. For *p*-FPhOH/TiO_2, the temporal changes in the intensity of the bands in this spectral region are not as pronounced as in the phenol case. Nonetheless, after 200 s the weak ν(C–O) band at 1265 cm^{-1} begins to decrease with a new equally weak band emerging at 1283 cm^{-1} and isosbestic points observable at 1278 and 1295 cm^{-1}. After ca. 200 s, a new band emerges at 1273 cm^{-1} for the *p*-BrPhOH/TiO_2 system with complete disappearance of the 1240 cm^{-1} (sh) and 1263 cm^{-1} bands (isosbestic points seen at 1267 cm^{-1} and 1287 cm^{-1}). By contrast, the infrared spectra of the *p*-ClPhOH/TiO_2 system reveal an initial loss of the bands at 1235 and 1259 cm^{-1} occurring after only 35 s with a new C–O stretching band emerging at 1283 cm^{-1}; isosbestic points are clearly visible at 1269 and 1297 cm^{-1}. In all four cases, a single intermediate is formed from the TiO_2 photo-assisted conversion of the phenol and *p*-halophenols. The data reported at the bottom of Table 2 provide some clues as to the nature of this new intermediate species. Examining the combined total point charge of the C_7=C_2–O_1 group in the phenolic structures shows that the magnitude of the negative point charges varies as PhOH > *p*-FPhOH ~ *p*-ClPhOH ≥ *p*-BrPhOH. Note that the measured point of zero charge (pzc) of TiO_2 is at pH 6.5 under our conditions, whereas the initial pHs of the *p*-XPhOH/TiO_2 dispersions ranged from pH 5.8 (*p*-FPhOH) to pH 6.2 (PhOH); the corresponding pKs are PhOH (10.0) > *p*-FPhOH (~9.8) > *p*-ClPhOH (~9.4) > *p*-BrPhOH (~9.3). Accordingly, the substrates adopt their hydroxylated form in the aqueous dispersions so that adsorption should follow a trend similar to the trend of the negative point charges. The corresponding radical frontier electron densities of the C_7=C_2–O_1 group (Table 2) vary according to PhOH > *p*-FPhOH > *p*-ClPhOH > *p*-BrPhOH. This suggests that attack by the photogenerated $^{\bullet}$OH radical should occur preferentially at this group, more precisely at the *C7* carbon position, to yield catechol in the case of PhOH and 4-halocatechols for the *p*-XPhOH substrates, in line with earlier reports [11,14,40–44].

3.3. Photo-assisted degradation and mineralization of the p-halophenols and phenol

An important influential factor for the initial photodegradation in aqueous TiO_2 dispersions depends on the expected position of $^{\bullet}$OH-radical attack as inferred from the radical frontier electron densities and from the data summarized in Table 2. A simple mechanism sees TiO_2 particles absorb UV light of energy greater than the band gap (ca. 3.2 eV by diffuse reflectance spectra, λ = 387.4 nm) to generate electron-hole pairs (reaction (1)). The holes (h^+) are ultimately trapped by surface HO^- ions or by adsorbed H_2O molecules on the TiO_2 particle surface to yield H^+ and $^{\bullet}$OH radicals (reaction (2)). Concomitantly, dioxygen molecules react with conduction band electrons (e_{cb}^-) to yield superoxide radical anions, $O_2^{\bullet -}$, which on protonation generates the hydroperoxy, $^{\bullet}$OOH, radicals (reactions (3a) and (3b)). These and possibly the photogenerated holes subsequently lead to photooxidation of the substrates (reactions (4a) and (4b), respectively):

$$TiO_2 + h\nu\,(\lambda = 387.4\,nm) \rightarrow TiO_2(e_{cb}^- + h_{vb}^+) \quad (1)$$

$$h_{vb}^+ + H_2O\,(\text{or } OH_{surf}^-) \rightarrow {}^{\bullet}OH + H^+ \quad (2)$$

$$e_{cb}^- + O_2\,(soln) \rightarrow O_2^{\bullet -} \quad (3a)$$

Table 2
Summary of the kinetics in the TiO_2-assisted photooxidation of *p*-XPhOH (X = H, F, Cl, Br), of phenol in the presence of halide ions and some calculated point charges and radical frontier electron densities

Parameters	*p*-ClPhOH	*p*-BrPhOH	*p*-FPhOH	PhOH
k_{deg} ($\times10^{-3}$ mM min^{-1})	2.27	2.65	2.20	2.32
k_{CO_2} ($\times10^{-2}$ min^{-1}) (induction period)	1.6 (15 min)	1.2 (15 min)	1.7 (30 min)	1.4 (10 min)
% CO_2	98	87	94	100
k_{X^-} ($\times10^{-2}$ min^{-1})	2.87	1.73	5.57	–
[X^-][a] (mM)	0.20	0.18	0.13	–

	k_{deg} ($\times10^{-3}$ mM min^{-1})
Phenol degradation in the presence of halide ions	
PhOH/Cl^-	1.70
PhOH/Br^-	0.62
PhOH/F^-	1.87
PhOH alone	1.78

	p-ClPhOH	*p*-BrPhOH	*p*-FPhOH	PhOH
Calculated point charges and radical frontier electron densities (RFED)[b]				
Point charges				
$C_7{=}C_2{-}O_1$[c]	−0.447	−0.441	−0.448	−0.482
X^-	−0.031	+0.045	−0.138	–
C_5	−0.136	−0.251	+0.025	−0.196
RFED				
$C_7{=}C_2{-}O_1$[c]	0.759	0.733	0.773	0.804
C_5	0.431	0.457	0.424	0.391
Electronegativity of X	2.83	2.74	4.1	–

[a] After 3 h of irradiation.
[b] Ref [26].
[c] Total point charges and radical frontier electron densities on these three atoms.

$$O_2^{\bullet-} + H^+ \rightarrow {}^{\bullet}OOH \quad (3b)$$

$$^{\bullet}OH\,(\text{or}\,^{\bullet}OOH) + \text{halophenol} \rightarrow\rightarrow \text{oxidation products} \quad (4a)$$

$$h_{vb}{}^+ + \text{halophenol} \rightarrow\rightarrow \text{oxidation products} \quad (4b)$$

Under our experimental conditions, the TiO_2 particle surface is positively charged resulting from an excess number of protons from the oxidation of H_2O (Eq. (2)) or from the acidic medium (see above). Accordingly, the $^{\bullet}OH$ radical photogenerated on the TiO_2 surface is expected to be a major oxidative agent [11,41,43,44] to attack the PhOH, *p*-FPhOH, *p*-ClPhOH and *p*-BrPhOH substrates at or near the TiO_2 surface (Scheme 1).

The temporal decrease of the concentration of the *p*-halophenols and phenol in aqueous TiO_2 dispersions, as witnessed by UV absorption spectroscopy, is illustrated in Fig. 4(a), whereas Fig. 4(b) reports the temporal changes in the pH of the dispersions during the photodegradation process. The pH changes tend toward more acidic media as a result of formation of acidic intermediates. However, such changes are tempered by the buffering action of the TiO_2 surface.

Under dark conditions, the initial adsorption of each substrate on the TiO_2 surface was less than ca. 4%. The zero-order rates of photodegradation are reported in Table 2. Note that *p*-BrPhOH degrades via first-order kinetics. Within experimental error, there appears to be relatively little variation in the photodegradation dynamics of the four substrates to intermediate products, with *p*-BrPhOH degrading slightly faster. In this regard, it is interesting to note that Lapertot et al. [23] found no correlation between adsorption of the *p*-halophenols on the TiO_2 surface and the photodegradation rates.

The TiO_2 photo-assisted mineralization of the substrates to carbon dioxide, illustrated in Fig. 5, required an induction period before evolution of CO_2 could be detected: *p*-FPhOH (30 min) > *p*-ClPhOH ∼ *p*-BrPhOH (15 min) > PhOH (10 min). First-order rates of formation of carbon dioxide follow the order *p*-FPhOH > *p*-ClPhOH > PhOH > *p*-BrPhOH (Table 2), which except for PhOH is in good accord with Hammettt's σ constants [45]. Photomineralization was quantitative for PhOH (100%) after 3 h of UV irradiation and nearly so for *p*-ClPhOH (98%) and *p*-FPhOH (94%); however, photomineralization of *p*-bromophenol was only ca. 87% complete after this period.

Formation of free F^-, Cl^-, and Br^- halide ions during the photomineralization of *p*-chlorophenol, *p*-bromophenol and *p*-fluorophenol is displayed in Fig. 6. The first-order rates of dehalogenation of the *p*-halophenols followed the trend *p*-FPhOH ≫ *p*-CPhOH > *p*-BrPhOH, a trend identical to the manner in which the negative point charges vary: *p*-FPhOH (−0.138) ≫ *p*-ClPhOH (−0.031) > *p*-BrPhOH (+0.045); see Table 2.

After the 3-h irradiation period, dechlorination was complete, whereas debromination was ca. 90% complete and only 65% of

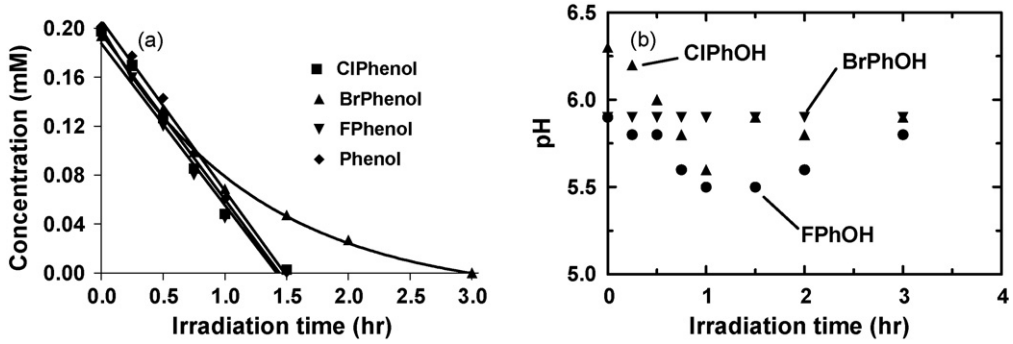

Fig. 4. (a) Plot showing the temporal loss of the *p*-chlorophenol (280 nm), *p*-bromophenol (280 nm), *p*-fluorophenol (277 nm) and phenol (270 nm) under UV illumination in air-equilibrated aqueous TiO_2 dispersions as determined by UV spectral methods. (b) Dependence of pH on irradiation time during the photodegradation of the halophenols.

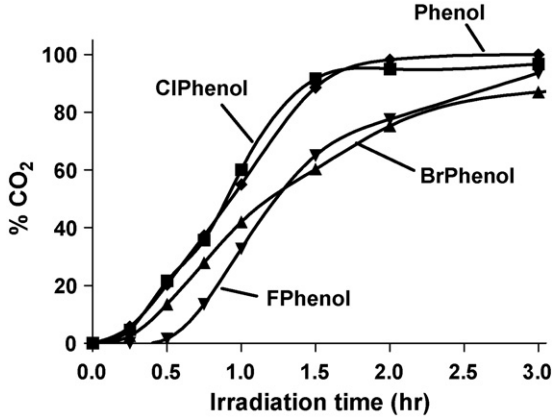

Fig. 5. CO_2 evolution in the photodegradation of phenol, *p*-florophenol, *p*-chlorophenol, and *p*-bromophenol in aqueous TiO_2 dispersion systems.

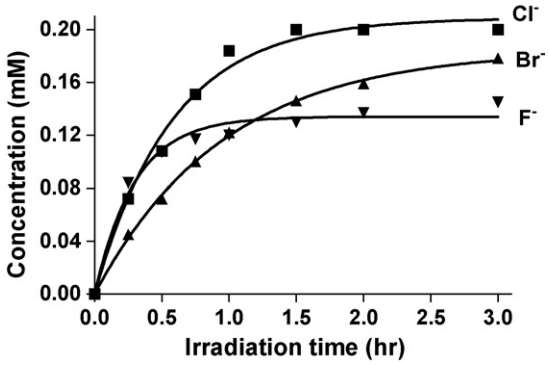

Fig. 6. Formation of F^-, Cl^-, and Br^- ions during the course of the photomineralization of *p*-fluorophenol, *p*-chlorophenol and *p*-bromophenol, respectively. Initial concentrations of the halophenols, 0.20 mM.

the F^- ions were recovered. The latter is consistent with earlier observations [41] that fluoride ions tend to remain strongly adsorbed on the TiO_2 particle surface. In addition, comparison of the kinetic data of CO_2 formation, k_{CO_2}, and those of dehalogenation, k_{X^-}, clearly indicates that dehalogenation precedes mineralization.

3.4. Influence of halide ions (F^-, Cl^-, Br^-) on the TiO_2 photo-assisted degradation of phenol

The influence of the halide ions on the photodegradation of PhOH was examined to clarify differences in the dynamics, i.e. variations in k_{deg} (if any) for each of the *p*-halophenols. The experimental procedure was described earlier in Section

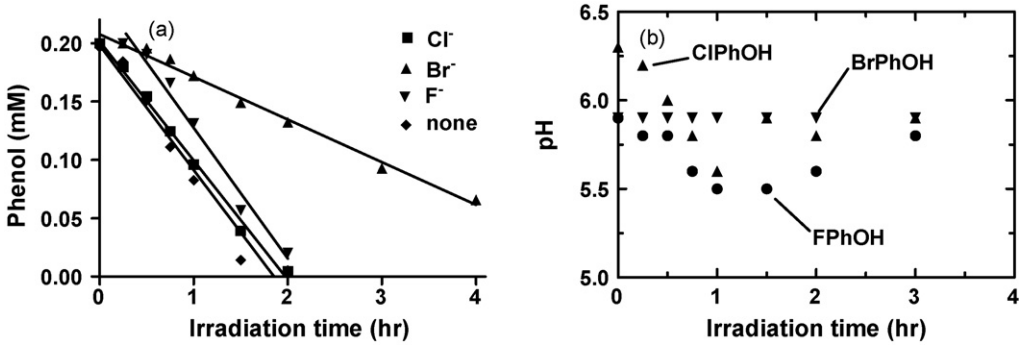

Fig. 7. (a) Plot showing the temporal loss of the phenol target pollutant substrate (0.20 mM) as determined by UV spectral methods; phenol/Cl^- ion: phenol solution containing 0.20 mM Cl^-, phenol/Br^- ion: phenol solution containing 0.20 mM Br^-; phenol/F^- ion: phenol solution containing 0.20 mM F^-. (b) Temporal changes in pH during the photodegradation of phenol in the presence of halide ions (0.20 mM).

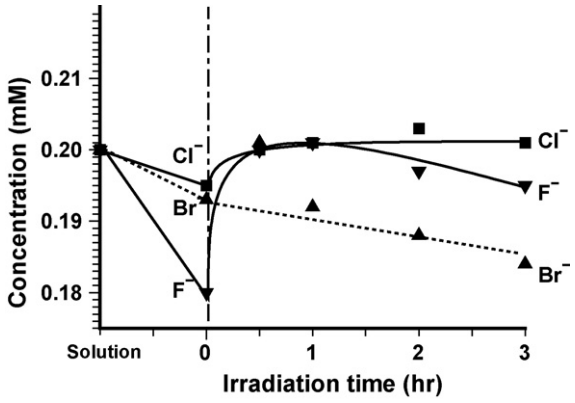

Fig. 8. Adsorption and photoadsorption behavior of the halide ions in TiO_2 dispersions in the dark and under UV irradiation, respectively.

2.2. Results from the TiO_2 photo-assisted degradation of phenol alone and in the presence of F^-, Cl^- and Br^- ions are depicted in Fig. 7(a). The relevant kinetics are summarized in Table 2. Fig. 7(b) displays the pH changes occurring during the photodegradation of phenol in the presence of the three halide ions.

Comparison of the kinetic data reveals no variations in the photodegradation kinetics of PhOH/F^- and PhOH/Cl^- with the kinetics of PhOH photodegradation, in contrast to a recent study by Calza et al. [46] who found a nearly twofold accelerating effect of the photodegradation of PhOH in the presence of F^- ions in P-25 TiO_2 suspensions and a threefold faster degradation in suspensions containing sol–gel TiO_2 prepared from titanium tetra-isopropoxide. The discrepancy with our results is due mostly to differences in fluoride ion concentration (10 mM versus 0.20 mM in our case) and to a pH effect. In the study of Calza et al. [46] the pH of the dispersion was set at 3.6 at which the fluorination of the P-25 TiO_2 particles surface was maximal. Surface coverage by fluoride ion is substantially less at about pH 6 [47]. Except for the Br/PhOH system (Fig. 7(b)) and for PhOH (Fig. 4(b)), for which the pHs remained constant throughout the photodegradative process, the pH did change somewhat for the Cl/PhOH and F/PhOH systems tending to decrease with irradiation time but returning to its initial value at the conclusion of the process. Under our conditions the pH effect was rather minimal.

The photodegradation of phenol was threefold slower in the presence of bromide ions. Evidently, the bromide ion either blocks the surface-active sites or otherwise competes with phenol for the $^{\bullet}OH$ radicals (or valence band holes), more so than chloride or fluoride, thereby inhibiting reactions (4a) and (4b).

Further examination of the role of the halide ions on the photodegradation process was necessary to understand their role in the trend(s) observed in Fig. 7(a). Results are presented in Fig. 8. Under dark conditions, all three halide ions adsorbed to some extent on the surface: F^- ($\sim$10%) > Br^- (3–4%) $\geq$ Cl^- (2–3%). Under irradiation, however, both F^- and Cl^- ions initially photodesorbed, whereas the Br^- ion was either further photoadsorbed or otherwise was being oxidized. No attempt was made to analyze this particular effect further. After ca. 1 h, the fluoride ion concentration decreased indicating some photoadsorption taking place, in contrast to the chloride ion which showed no changes. These results confirm our earlier inference that the lower photodegradation efficiency of the phenol/Br^- ion system in Fig. 7(a) was caused either by the blocking of surface-active sites by the bulky bromide ions or otherwise the Br^- underwent competitive oxidation with the phenol substrate [48].

4. Concluding remarks

DRIFT spectral results reported herein have shown that some degree of adsorption and photoadsorption takes place when the *p*-halophenols and phenol interact with the metal-oxide particle surface, albeit in the dark the extent of adsorption is less than ca. 4%. More importantly, irradiation of the *p*-XPhOH/TiO_2 specimens has shown that a single intermediate forms initially under very weak irradiation conditions as available from laboratory ceiling fluorescent lamps. The primary intermediates have been identified as catechol in the case of phenol and the 4-halocatechols for the *p*-XPhOH substrates (X = F, Cl, Br). TiO_2 photo-assisted dehalogenation and mineralization are nearly quantitative with the former preceding the latter. Calculated point charges and radical frontier electron densities of all the atoms in the phenolic structures have aided in inferring the mode of adsorption and the subsequent most plausible position of attack of the phenyl ring by the photogenerated $^{\bullet}OH$ radicals. With very few exceptions, we found no correlation between the extent of adsorption or photoadsorption of the *p*-XPhOH (X = H, F, Cl, Br) substrates and the photodegradation or photomineralization dynamics, thus confirming the earlier observations reported by Lapertot et al. [23].

Acknowledgments

We are grateful to the Sophia University-wide Collaborative Research Fund, the Foundation of Research for Promoting Technological Seeds from the Japan Science and Technology Agency and the Foundation of Sasakawa Scientific Research Grant from the Japan Science Society for financial support to SH. The studies in Pavia were supported by a grant from the Ministero dell'Università e Ricerca (MUR-Roma). NS is particularly grateful to Prof. Albini and his group for their gracious hospitality during his stay in Pavia. We also wish to thank the personnel of the JASCO Co. Ltd. for the analytical support and assistance with the HPLC and FT-IR operations.

References

[1] M.R. Hoffmann, S.T. Martin, W. Choi, D.W. Bahnemann, Chem. Rev. 95 (1995) 69.
[2] K. Vinodgopa1, U. Stafford, K.A. Gray, P.V. Kamat, J. Phys. Chem. 98 (1994) 6797.
[3] D. Fabbri, A. Bianco Prevot, E. Pramauro, Appl. Catal. B: Environ. 62 (2006) 21.
[4] N.J. Peill, M.R. Hoffmann, Environ. Sci. Technol. 30 (1996) 2806.
[5] Z. Ai, P. Yang, X. Lu, J. Hazard. Mater. B124 (2005) 147.

[6] S. Horikoshi, A. Tokunaga, N. Watanabe, H. Hidaka, N. Serpone, J. Photochem. Photobiol. A: Chem. 177 (2006) 129.
[7] D.W. Bahnemann, Solar Energy 77 (2004) 445.
[8] A. Mills, J. Wang, J. Photochem. Photobiol. A: Chem. 118 (1998) 53.
[9] P. Boule, C. Guyon, J. Lemaire, Toxicol. Environ. Chem. 7 (1984) 97.
[10] J.-C. D'Oliveira, G. Al-Sayyed, P. Pichat, Environ. Sci. Technol. 24 (1990) 990.
[11] A. Mills, S. Morris, R. Davies, J. Photochem. Photobiol. A: Chem. 70 (1993) 183.
[12] J.-C. D'Oliveira, C. Minero, E. Pelizzetti, P. Pichat, J. Photochem. Photobiol. A: Chem. 72 (1993) 26.
[13] S. Martin, A. Lee, M.R. Hoffmann, Environ. Sci. Technol. 29 (1995) 2567.
[14] J. Theurich, M. Lindner, D.W. Bahnemann, Langmuir 12 (1996) 6368.
[15] X. Li, J.W. Cubbage, T.A. Tetzlaff, W.S. Jenks, J. Org. Chem. 64 (1999) 8509.
[16] X. Li, J.W. Cubbage, W.S. Jenks, J. Org. Chem. 64 (1999) 8525.
[17] U. Stafford, K.A. Gray, P.V. Kamat, A. Varma, Chem. Phys. Lett. 205 (1993) 55.
[18] A.V. Emeline, A. Salinaro, N. Serpone, J. Phys. Chem. B 104 (2000) 11202.
[19] A.V. Emeline, N. Serpone, J. Phys. Chem. B 106 (2002) 12221.
[20] D.C. Hurum, K.A. Gray, T. Rajh, M.C. Thurnauer, J. Phys. Chem. B 108 (2004) 16483.
[21] N. Serpone, R. Terzian, H. Hidaka, E. Pelizzetti, J. Phys. Chem. 98 (1994) 2634.
[22] K.E. O'Shea, C. Cardona, J. Org. Chem. 59 (1994) 5005.
[23] M. Lapertot, P. Pichat, S. Parra, C. Guillard, C. Pulgarin, J. Environ. Sci. Health, Part A 41 (2006) 1009.
[24] R. Nakamura, A. Imanishi, K. Murakoshi, Y. Nakato, J. Am. Chem. Soc. 125 (2003) 7443.
[25] A. Klamt, G. Schuurmann, J. Chem. Soc. Perkin Trans. 2 (1993) 799.
[26] A complete set of point charges and radical frontier electron densities calculated for all the atoms in the four phenolic structures reported herein (*p*-X-PhOH, X = H, F, Cl, Br) is available upon request from one of the authors: s-horiko@sophia.ac.jp.
[27] W. Zierkiewicz, D. Michalska, B. Czarnik-Matusewicz, M. Rospenk, J. Phys. Chem. A 107 (2003) 4547.
[28] W. Zierkiewicz, D. Michalska, T. Zeegers-Huyskens, J. Phys. Chem. A 104 (2000) 11685.
[29] (a) A.R. Nicolaescu, O. Wiest, P.V. Kamat, J. Phys. Chem. A 109 (2005) 2822;
(b) A.R. Nicolaescu, O. Wiest, P.V. Kamat, J. Phys. Chem. A 109 (2005) 2829;
(c) J. Peller, O. Wiest, P.V. Kamat, J. Phys. Chem. A 108 (2004) 10925.
[30] B. Azambre, O. Heintz, D. Robert, J. Zawadzki, J.V. Weber, Environ. Chem. (2005) 19.
[31] M.A. Blesa, A.D. Weisz, P.J. Morando, J.A. Salfity, G.E. Magaz, A.E. Regazzoni, Coord. Chem. Rev. 196 (2000) 31.
[32] A.D. Weisz, L. Garcia-Rodenas, P.J. Morando, A.E. Regazzoni, M.A. Blesa, Catal. Today 76 (2002) 103.
[33] A.D. Weisz, A.E. Regazzoni, M.A. Blesa, Solid State Ionics 143 (2001) 125.
[34] S.J. Hug, D.W. Bahnemann, J. Electron Spectros. Related Phenom. 150 (2006) 206.
[35] (a) J.R.S. Brownson, M.I. Tejedor-Tejedor, M.A. Anderson, J. Phys. Chem. B 110 (2006) 12494;
(b) J.R.S. Brownson, M.I. Tejedor-Tejedor, M.A. Anderson, Chem. Mater. 17 (2005) 6304.
[36] C.B. Mendive, D.W. Bahnemann, M.A. Blesa, Catal. Today 101 (2005) 237.
[37] D. Michalska, W. Zierkiewicz, D.C. Bienko, W. Wojciechowski, T. Zeegers-Huyskens, J. Phys. Chem. A 105 (2001) 8734.
[38] U. Gesenhues, J. Phys. Chem. Solids 68 (2007) 224.
[39] A. Kraynov, R. Richards, Phys. Chem. Chem. Phys. 9 (2007) 884.
[40] C. Dong, C.-W. Chen, S.-S. Wu, Hazard. Ind. Wastes 27 (1995) 361.
[41] C. Minero, C. Aliberti, E. Pelizzetti, R. Terzian, N. Serpone, Langmuir 7 (1991) 928.
[42] G. Al-Sayyed, G.C. D'Oliveira, P. Pichat, J. Photochem. Photobiol. A: Chem. 58 (1991) 99.
[43] C.-D. Dong, C.-P. Huang, Trace Met. Environ. 3 (1993) 701 (photocatalytic purification and treatment of water and air).
[44] C.-D. Dong, C.-P. Huang, Adv. Chem. Ser. 244 (1995) 291.
[45] S. Parra, J. Olivero, L. Pacheco, C. Pulgarin, Appl. Catal. B: Environ. 43 (2003) 293.
[46] P. Calza, E. Pelizzetti, K. Mogyorosi, R. Kun, I. Dekany, Appl. Catal. B: Environ. 72 (2007) 314.
[47] C. Minero, G. Mariella, V. Maurino, E. Pelizzetti, Langmuir 16 (2000) 2632.
[48] R. Nakamura, T. Tanaka, Y. Nakato, J. Phys. Chem. B 109 (2005) 8920.